

# Nonequilibrium effects in hadronic fireball expansion

L.M. Satarov<sup>1,2</sup>, A.B. Larionov<sup>2,3</sup>, and I.N. Mishustin<sup>1,2</sup>

<sup>1</sup> *Frankfurt Institute for Advanced Studies, D-60438 Frankfurt am Main, Germany*

<sup>2</sup> *National Research Center "Kurchatov Institute", 123182 Moscow, Russia*

<sup>3</sup> *Institut für Theoretische Physik, Universität Giessen, D-35392 Giessen, Germany*

## Abstract

We consider a spherical volume of hot and dense hadronic matter (fireball) expanding into a vacuum. It is assumed that initially the fireball matter is in local thermal and chemical equilibrium with vanishing collective velocity. The time evolution of the fireball is studied in parallel within the GiBUU transport model and an ideal hydrodynamic model. The equation of state of an ideal hadronic gas is used in the hydrodynamic calculation. The same set of hadronic species is used in transport and fluid-dynamical simulations. Initial coordinates and momenta of hadrons in transport simulations have been randomly generated by using the Fermi and Bose distributions for (anti)baryons and mesons. The model results for radial profiles of densities and collective velocities of different hadronic species are compared at different times. We find that two considered models predict essential differences in time evolution of hadron abundances, which are especially pronounced for hyperonic species. This gives an evidence of a strong deviation from chemical equilibrium in expanding hadronic matter.

PACS numbers: 24.10.Lx, 24.10.Nz, 25.75.Dw, 25.75.Ld

## I. INTRODUCTION

Physics of high energy heavy-ion collisions exhibits a rapid development during last several decades. A lot of efforts has been made to extract the information on properties of hot and dense nuclear matter from experimental data. Numerous theoretical models have been proposed to describe the complicated dynamics of multi-particle systems produced in nuclear collisions. An important place in understanding the main features of experimental data is still occupied by simple fireball [1, 2], blast wave [3, 4] and thermal [5, 6] models.

More sophisticated hydrodynamic models (see e.g. a recent review [7]) have been very successful in reproducing a large amount of experimental data in a wide range of bombarding energies. An attractive feature of these models is their capability to study the sensitivity of observables to the equation of state (EoS) of strongly interacting matter and, in particular, to a possible deconfinement phase transition. The hydrodynamic models (HDM) are usually applied to describe the evolution of matter only at some intermediate stage of a heavy-ion collision. They are not well suited for early and late stages since large deviations from local thermodynamic equilibrium are expected in this case.

As a rule, these models assume the formation of a quasi-equilibrated fireball at an intermediate stage of the collision process. The geometrical and thermodynamic parameters of the initial fireball are normally chosen to achieve the best fit of observed data. The (2+1)-dimensional HDM [8–12] became especially popular in recent years. These models describe the dynamics of a cylindrical fireball expanding in transverse and longitudinal directions.

Of course, the hydrodynamic approach can not be directly applied to simulate the late stages of a heavy-ion reaction when collisions of particles become too rare to maintain the thermodynamic equilibrium. The assumption of an instantaneous transition to the collisionless propagation of particles ("freeze-out") has been introduced [13, 14] to calculate the asymptotic particle spectra in HDM. However, the direct kinetic simulations of space-time distributions of last-collision points in relativistic nuclear reactions show [15] that the freeze-out is in fact a continuous process, even in central interactions of heaviest nuclei (for details, see [7, 16]). It has been also conjectured [17, 18] that the stages of a "chemical" (saturation of particle multiplicities) and "kinetic" (saturation of particle spectra) freeze-out should be separated in time. It is believed that the chemical freeze-out takes place earlier because of much faster drop of inelastic collision rates as compared to elastic ones

in expanding matter. On the other hand, there are several fluid-dynamical studies [19, 20] where experimental particle spectra have been successfully reproduced without introducing such a separation.

Thermodynamic equilibrium is not postulated in microscopic transport models of nuclear collisions. Currently, the UrQMD [21], GiBUU [22, 23], HSD [24, 25], QGSM [26] and AMPT [27] transport models are widely used for simulating relativistic nuclear collisions. These models are not well suited for describing high density states of hadronic matter, where multiparticle (non-binary) channels of hadronic interactions are presumably important. As a rule, contributions of such channels are disregarded in existing versions of transport models. On the other hand, as demonstrated in Refs. [28–30], multimesonic channels of baryon–antibaryon pair production might be responsible for high yields of antiprotons and antihyperons observed at SPS and RHIC energies.

A more realistic description of the freeze-out processes in heavy-ion collisions can be achieved in a hybrid "hydro-cascade" model [11, 12, 31–33]. In this approach, hydrodynamic and cascade simulations are applied, respectively, for intermediate and late stages of the reaction. The hybrid model implicitly assumes the existence of a space-time region where the hydrodynamic and cascade simulations give similar results. The characteristics of hydrodynamic flow taken at a certain hypersurface are used for generating phase-space coordinates of hadrons which serve as an input for subsequent transport simulations.

Although such a procedure seems to be intuitively justified, it should be verified for more or less typical situations. In the present work, a spherical expansion of an ideal hadronic gas is simulated in parallel by using the transport and hydrodynamic models. Specifically we use a non-viscous hydrodynamics with an ideal-gas EoS and the transport GiBUU model [22, 23] (without mean-field interactions). The initial fireball is assumed to be in thermodynamic equilibrium. Thermodynamic parameters of this state are used to generate randomly the set of initial hadrons for subsequent transport calculations. By the direct comparison of results predicted by the GiBUU and HDM we investigate possible deviations from thermal and chemical equilibrium in the course of expansion.

Finally, we would like to mention several earlier works [34–36] which studied the particle composition in an expanding fireball within a "hadrochemical" approach. There a set of rate equations for particle abundances was combined with a simplified hydrodynamic description. But the calculations had been performed for a spatially uniform background neglecting

surface effects. The direct comparison between hydrodynamic and transport calculations have been recently made in the case of a cylindrical gluonic fireball in Ref. [37]

The paper is organized as follows: parameters of the initial fireball are given in Sec. IIA, our hydrodynamic model is formulated in Sec. IIB. In this section we also show radial profiles of densities and collective velocities obtained by numerical solution of fluid-dynamical equations. Our transport model is formulated in Sec. IIC. In Sec. III we compare the predictions of the hydrodynamic and transport models. Our conclusions are presented in Sec. IV. The procedure of initial event generation is described in Appendix.

## II. DESCRIPTION OF THE MODELS

### A. Initial state

We assume that at  $t = 0$  the fireball is locally equilibrated and has vanishing collective velocity. The initial radial profiles of energy ( $\varepsilon$ ) and baryon ( $n$ ) densities are parametrized by the Woods–Saxon distribution with some radius  $R$  and diffuseness  $a$ :

$$\varepsilon(r, 0) = \varepsilon_0 W(r), \quad n(r, 0) = n_0 W(r), \quad W(r) = \left[ \exp\left(\frac{r - R}{a}\right) + 1 \right]^{-1}. \quad (1)$$

Below we choose the following parameters:

$$R = 6 \text{ fm}, a = 0.3 \text{ fm}, \varepsilon_0 = 1.3 \text{ GeV/fm}^3, n_0 = 0.45 \text{ fm}^{-3}. \quad (2)$$

The initial values of energy and baryon densities at the fireball center,  $\varepsilon_0$  and  $n_0$ , are typical for high density states of hadronic matter created in heavy-ion collisions at  $E_{\text{lab}} \simeq 10 \text{ AGeV}$  (see e.g. Ref. [38]).

### B. Hydrodynamic simulation of fireball expansion

In this section we describe the HDM for simulating the fireball expansion. The model assumes that deviations from local equilibrium are small at any space-time point  $(\mathbf{r}, t)$ . In this approximation, the single-particle phase-space distribution function (DF) of  $i$ -th hadronic species is equal to a locally equilibrated DF  $f_i^{(eq)}$  characterized by certain temperature  $T$ ,

chemical potential  $\mu_i$  and collective 3-velocity  $\mathbf{v}$ . Considering the hadronic system as a mixture of ideal gases of (anti)baryons and mesons, one can approximate  $f_i^{(eq)}$  by the Fermi or Bose DF ( $\hbar = c = 1$ ):

$$f_i^{(eq)}(\mathbf{r}, \mathbf{p}, t) = \frac{g_i}{(2\pi)^3} \left[ \exp \left( \frac{\tilde{E}_i - \mu_i}{T} \right) \pm 1 \right]^{-1}, \quad (3)$$

where  $g_i$  is the spin-isospin degeneracy of  $i$ -th hadronic species [54],  $\tilde{E}_i = \gamma(E_i - \mathbf{p}\mathbf{v})$  is a single-particle energy in the local rest frame (LRF),  $E_i = \sqrt{m_i^2 + \mathbf{p}^2}$  is the corresponding energy in an arbitrary frame,  $m_i$  is the mass of  $i$ -th hadrons, and  $\gamma = (1 - \mathbf{v}^2)^{-1/2}$ . Plus or minus in the r.h.s. of Eq. (3) correspond, respectively, to fermions or bosons.

In our fluid-dynamical calculations we assume a fireball matter to be in chemical equilibrium with respect to strong interactions and decays of hadrons. In this case,  $\mu_i$  may be represented by linear combinations of the baryon ( $\mu$ ) and strange ( $\mu_S$ ) chemical potentials:

$$\mu_i = B_i\mu + S_i\mu_S, \quad (4)$$

where  $B_i = 0, \pm 1$  and  $S_i = 0, \pm 1, \pm 2 \dots$  are, respectively, the baryon and strangeness quantum numbers of the  $i$ -th hadrons.

The values of the net baryon ( $n$ ), strangeness ( $n_S$ ) and energy ( $\varepsilon$ ) densities in LRF, as well as pressure ( $P$ ) may be expressed [39] in terms of integrals of the DF (3) over the 3-momentum in this frame:

$$\begin{pmatrix} n \\ n_S \\ \varepsilon \\ P \end{pmatrix} = \sum_i \int d^3\tilde{p} \begin{pmatrix} B_i \\ S_i \\ \tilde{E}_i \\ \frac{\tilde{p}^2}{3\tilde{E}_i} \end{pmatrix} f_i^{(eq)}, \quad (5)$$

where the sum is taken over all hadronic species. Assuming that the strangeness density  $n_S = 0$  at any space-time point, and using Eqs. (3)–(5), one can express all thermodynamic quantities (e.g.  $T, \mu, \mu_S, P$ ) in terms of two independent variables  $n$  and  $\varepsilon$ . In particular, in this way we obtain the EoS of the fireball matter,  $P = P(n, \varepsilon)$ , which is used in our HDM (see below).

To facilitate the comparison with transport simulations, in our hydrodynamic calculations we use the EoS with the same set of hadrons and hadronic resonances as in the GiBUU model (see Appendix A of Ref. [23]). The set of nonstrange baryons ( $B_i = 1, S_i = 0$ )

TABLE I: Hadronic species included in the calculation.

hadron	$m_i$ (GeV)	$B_i$	$S_i$	$I_i$	$g_i$	$N_i$	$N_{\bar{i}}$	hadron	$m_i$ (GeV)	$B_i$	$S_i$	$I_i$	$g_i$	$N_i$	$N_{\bar{i}}$
$\pi$	0.140	0	0	1	3	256.9		$\Delta(1600)$	1.600	1	0	3/2	16	19.0	0.46
$K$	0.496	0	1	1/2	2	94.0		$\Delta(1620)$	1.630	1	0	3/2	8	8.2	0.20
$\overline{K}$	0.496	0	-1	1/2	2	28.4		$N(1650)$	1.655	1	0	1/2	4	3.6	0.089
$\eta$	0.543	0	0	0	1	21.4		$\Sigma(1660)$	1.660	1	-1	1	6	2.9	0.24
$\rho$	0.776	0	0	1	9	73.6		$\Lambda(1670)$	1.670	1	-1	0	2	0.93	0.076
$\omega$	0.782	0	0	0	3	23.9		$\Sigma(1670)$	1.670	1	-1	1	12	5.6	0.50
$\sigma$	0.800	0	0	0	1	7.4		$\Omega^-$	1.672	1	-3	0	4	0.55	0.50
$K^*$	0.892	0	1	1/2	6	53.9		$N(1675)$	1.675	1	0	1/2	12	8.9	0.24
$\overline{K}^*$	0.892	0	-1	1/2	6	16.3		$N(1680)$	1.685	1	0	1/2	12	9.4	0.23
$N$	0.939	1	0	1/2	4	107.6	2.5	$\Lambda(1690)$	1.690	1	-1	0	4	1.7	0.14
$\eta'$	0.958	0	0	0	1	3.7		$N(1700)$	1.700	1	0	1/2	8	5.8	0.14
$\phi$	1.020	0	0	0	3	8.4		$\Sigma(1750)$	1.750	1	-1	1	6	1.9	0.15
$\Lambda$	1.116	1	-1	0	2	13.2	1.0	$\Sigma(1775)$	1.775	1	-1	1	18	5.0	0.41
$\Sigma$	1.189	1	-1	1	6	28.1	2.2	$\Lambda(1800)$	1.800	1	-1	0	2	0.49	0.040
$\Delta$	1.232	1	0	3/2	16	110.6	2.6	$\Lambda(1810)$	1.810	1	-1	0	2	0.47	0.038
$\Xi$	1.315	1	-2	1/2	4	5.7	1.5	$\Lambda(1820)$	1.820	1	-1	0	6	1.3	0.11
$\Sigma(1385)$	1.385	1	-1	1	12	22.1	1.8	$\Lambda(1830)$	1.830	1	-1	0	6	1.3	0.10
$\Lambda(1405)$	1.406	1	-1	0	2	3.3	0.27	$N(1880)$	1.880	1	0	1/2	8	2.4	0.059
$N(1440)$	1.440	1	0	1/2	4	10.3	0.25	$\Lambda(1890)$	1.890	1	-1	0	4	0.63	0.052
$\Lambda(1520)$	1.520	1	-1	0	4	3.8	0.31	$\Delta(1905)$	1.890	1	0	3/2	24	6.9	0.17
$N(1520)$	1.520	1	0	1/2	8	14.0	0.34	$\Delta(1910)$	1.910	1	0	3/2	8	2.1	0.051
$\Xi(1530)$	1.533	1	-2	1/2	8	4.0	1.1	$\Sigma(1915)$	1.915	1	-1	1	18	2.5	0.21
$N(1535)$	1.530	1	0	1/2	4	6.7	1.6	$\Delta(1930)$	1.960	1	0	3/2	24	4.8	0.12
$\Lambda(1600)$	1.600	1	-1	0	2	1.3	0.11	$\Delta(1950)$	1.930	1	0	3/2	32	7.5	0.19

includes nucleons ( $N$ ), isobars ( $\Delta(1232)$ ) and their excited states. We also take into account hyperons stable with respect to strong decays ( $Y = \Lambda, \Sigma, \Xi, \Omega^-$ ) and hyperonic resonances ( $Y^* = \Sigma(1385), \Lambda(1405), \dots$ ). In addition to baryons we include corresponding antibaryons ( $B_i = -1$ ). The mesonic set ( $B_i = 0$ ) consists of stable mesons  $\pi, K, \overline{K}, \eta, \eta'$  and resonances  $\rho, \omega, \sigma, \varphi, K^*, \overline{K}^*$ .

The list of baryons and mesons included in our calculations is given in Table I [55]. The thermodynamic properties of a fireball matter, in particular, its EoS, are obtained assuming zero widths of resonances. Using Eqs. (1)–(5) and characteristics of hadrons from Table I we calculate the initial radial profiles of temperature  $T$ , chemical potentials  $\mu, \mu_S$  and partial densities of hadronic species,  $n_i = \int d^3\tilde{p} f_i^{(eq)}$ . This calculation gives the values  $T \simeq 180$  MeV,  $\mu \simeq 328$  MeV,  $\mu_S \simeq 110$  MeV at the fireball center ( $r = 0$ ). The last two columns of Table I show the equilibrium multiplicities of  $i$ -th hadrons ( $N_i$ ) and antibaryons ( $N_{\bar{i}}$ ) in the initial state. These quantities are obtained by the volume integration of the corresponding partial densities. One can see that most abundant

hadrons at  $t = 0$  are pions, nucleons and isobars. The total multiplicity of initial antibaryons (approximately 18.6) is much smaller than the total baryon number of the fireball  $B_{\text{tot}} = \sum_i |B_i|(N_i - N_{\bar{i}}) = \int d^3r n\gamma \simeq 417$ .

To describe the dynamics of spherical fireball expansion, we solve the equations of the (1+1)-dimensional ideal hydrodynamics. They can be written in the form [40]:

$$\frac{\partial \mathcal{N}}{\partial t} + \left( \frac{\partial}{\partial r} + \frac{2}{r} \right) (v\mathcal{N}) = 0, \quad (6)$$

$$\frac{\partial E}{\partial t} + \left( \frac{\partial}{\partial r} + \frac{2}{r} \right) M = 0, \quad (7)$$

$$\frac{\partial M}{\partial t} + \left( \frac{\partial}{\partial r} + \frac{2}{r} \right) (vM + P) = 0. \quad (8)$$

Here  $v = \mathbf{v}\mathbf{r}/r$  is the radial component of fluid velocity,  $\mathcal{N} = n\gamma$  is the net baryon density in the fireball c.m. frame,  $E$  and  $M$  are the components of the energy-momentum tensor:

$$E = T^{00} = \gamma^2(\varepsilon + v^2P), \quad M = T^{0r} = v(E + P). \quad (9)$$

The initial conditions for these equations are given by the relations (1) and  $v(r, 0) = 0$ . Solving (6)–(9) together with the EoS  $P = P(n, \varepsilon)$  gives the radial profiles of  $n, \varepsilon, v$  at fixed  $t > 0$ . Similar hydrodynamic studies of a spherical fireball expansion by using simplified EoSs have been performed earlier in Refs. [41–43].

The numerical solution of Eqs. (6)–(8) has been obtained by using the flux-corrected transport algorithm SHASTA [44, 45]. Typically, we choose the cell sizes  $\Delta r = 2.5 \cdot 10^{-2}$  fm,  $\Delta t = 5 \cdot 10^{-3}$  fm/c of the  $(r, t)$  grid. Similarly to Ref. [38], in this calculation we use linear interpolations of the  $P(n, \varepsilon)$  table prepared with fixed steps in  $n$  and  $\varepsilon$ . We have checked that our numerical scheme conserves the total baryon number, energy and entropy of the fireball with relative accuracy better than 1%.

The radial profiles of fluid-dynamical quantities calculated for different times  $t$  within the HDM are shown in Figs. 1–2. In particular, thick and thin lines in the left panel of Fig. 1 show the profiles of  $n$  and  $\mathcal{N}$ , respectively. As one can see in Fig. 1, a rarefaction wave propagates from the fireball periphery and reaches the fireball center at  $t \sim 10$  fm/c. At later times the matter in the whole fireball is involved in the expansion. At such times the radial profile of collective velocity can be approximated as  $v = Hr^\alpha$  with  $\alpha < 1$ . In Fig. 2, we do not show external parts of velocity profiles corresponding to dilute regions of matter with  $n < 10^{-3} \text{ fm}^{-3}$ . These parts certainly can not be realistically described within the ideal HDM because of large local Knudsen numbers.

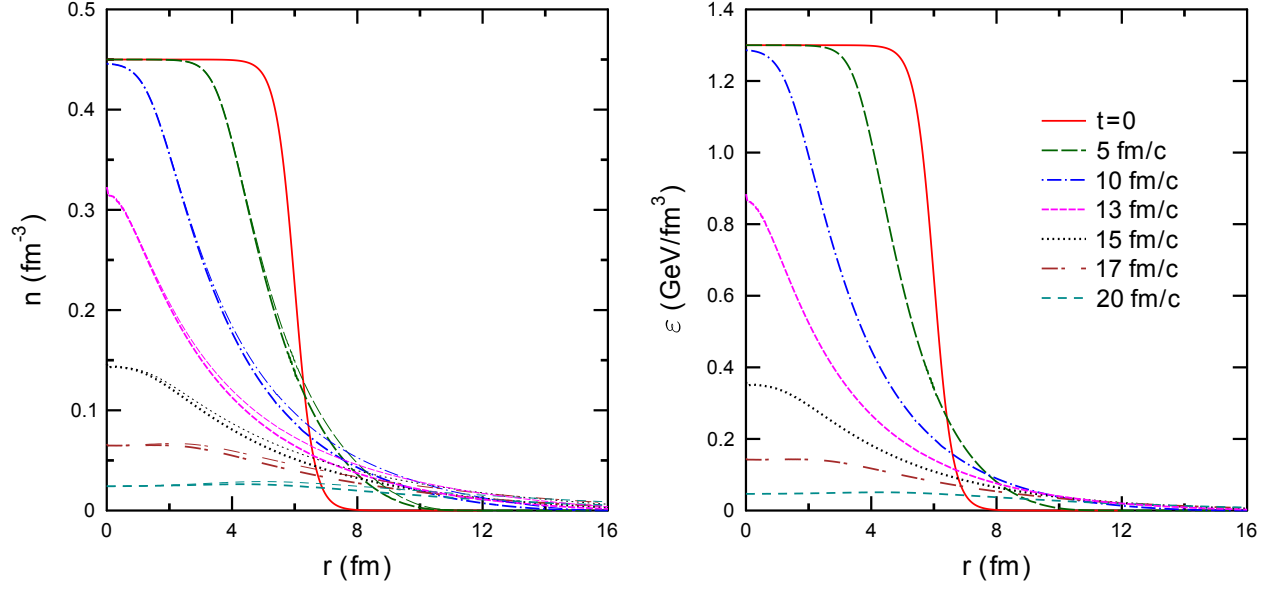


FIG. 1: The radial profiles of the baryon density (left panel) and energy density (right panel) calculated within HDM.

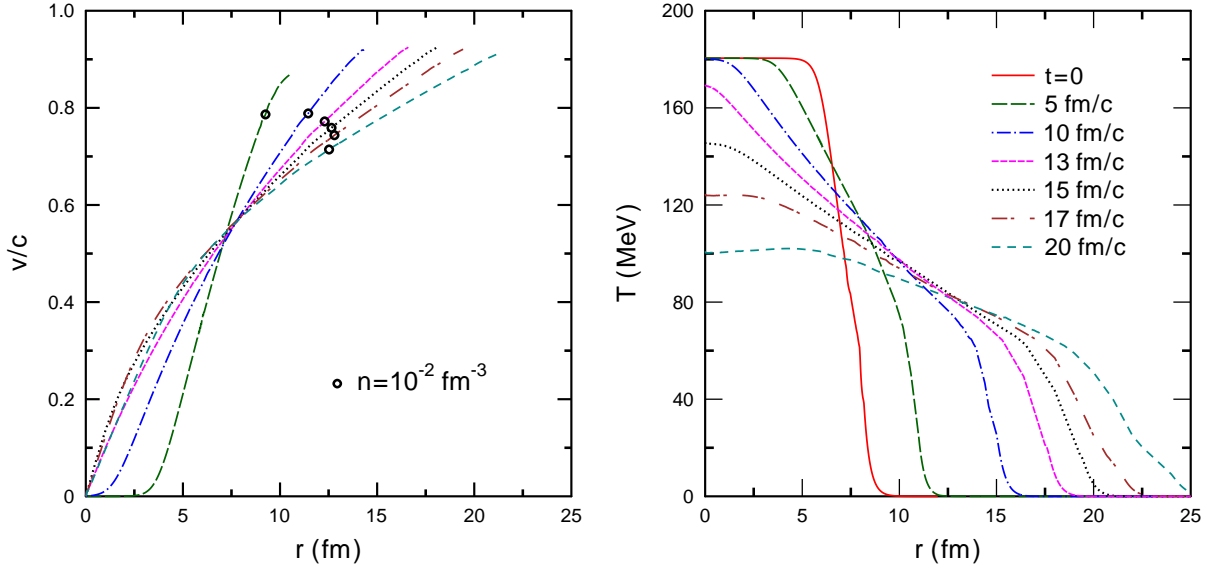


FIG. 2: The radial profiles of the collective velocity (left panel) and temperature (right panel) calculated in HDM. The outer parts of velocity profiles corresponding to densities  $n < 10^{-3} \text{ fm}^{-3}$  are omitted. The dots in the left panel correspond to spatial points where  $n = 10^{-2} \text{ fm}^{-3}$ .



### C. The GiBUU transport model

To study possible deviations from local equilibrium, the expansion of the hadronic fireball has been also simulated within the GiBUU transport model (version 1.2.2) [22, 23, 46]. The detailed description of the model is given in Ref. [23], below we present only its short summary. We apply GiBUU in a cascade mode, i.e. omitting contributions of nuclear and Coulomb potentials. The evolution of hadronic phase-space DFs  $f_i(\mathbf{r}, \mathbf{p}, t)$  due to free propagation of hadrons, as well as due to their two-body collisions and resonance decays is described by kinetic equations with corresponding collision terms. They are solved by using the standard test-particle method [47] which includes the Hamiltonian equations of motions for test particles and their two-body collisions (or decays) generated by a Monte Carlo method. In present calculations we use one test particle per hadron and consider a large number of parallel ensembles which we call "events". Each event is characterized by a specific sets of hadronic species, as well as their coordinates  $\mathbf{r}_j(t)$  and momenta  $\mathbf{p}_j(t)$ .

The DF of  $i$ -th hadronic species is represented as follows

$$f_i(\mathbf{r}, \mathbf{p}, t) = \left\langle \sum_{j=1}^{N_i} \delta[\mathbf{r} - \mathbf{r}_j(t)] \delta[\mathbf{p} - \mathbf{p}_j(t)] \right\rangle, \quad (10)$$

where the angular brackets denote averaging over all events and the sum runs over all hadrons of the type  $i$  existing at given time  $t$  in a given event [56]. The hadrons propagate along straight-line trajectories ( $\dot{\mathbf{r}}_j = \mathbf{p}_j/E_j$ ,  $\dot{\mathbf{p}}_j = 0$ ) between their two-body scatterings. The latter change the momenta abruptly and also lead to production of new hadrons [57]. Resonances are allowed to decay during time evolution.

For calculating collective velocities of particles, one should know radial profiles of the 4-current density  $J_i^\mu$  and the energy-momentum tensor  $T_i^{\mu\nu}$  of the hadronic species  $i$ . As in the HDM, we consider initial states with spherically symmetric distributions of particles. Let us consider a thin shell occupying a region of points with radii between  $r$  and  $r + \Delta r$ . In the spherical coordinate system with the origin at the fireball center, only the components of  $J_i^\mu, T_i^{\mu\nu}$  with  $\mu, \nu = 0, r$  are nonzero in the limit of a large number of events. By using Eq. (10)

one can get the relations:

$$J_i^0(r, t) = \int d^3p f_i = \left\langle \sum_{j=1}^{N_i} \Theta_j \right\rangle, \quad (11)$$

$$T_i^{00}(r, t) = \int d^3p E_i f_i = \left\langle \sum_{j=1}^{N_i} E_j \Theta_j \right\rangle, \quad (12)$$

where  $\Theta_j = (4\pi r^2 \Delta r)^{-1}$  if the radial coordinate  $r_j$  of hadron  $j$  in a given event falls into the interval  $(r, r + \Delta r)$  and  $\Theta_j = 0$  in the opposite case. The second equalities in (11)–(12) are obtained in the limit of small  $\Delta r$  and large number of events. A similar expression for  $J_i^r$  takes place after replacing  $\Theta_j \rightarrow v_j^r \Theta_j$  in (11), where  $v_j^r$  is the radial component of the  $j$ -th hadron velocity. The replacements of  $\Theta_j$  by  $v_j^r \Theta_j$  and  $(v_j^r)^2 \Theta_j$  in (12) give, respectively, the corresponding relations for  $T_i^{0r}$  and  $T_i^{rr}$ .

For generating initial events we use a procedure similar to that suggested in Ref. [33]. It is described in Appendix. These events have been generated according to the Fermi and Bose DF of hadrons (3). In principle, in this way one should obtain the same ensemble averaged initial distributions in both models [58]. Unless otherwise stated, the GiBUU simulations are averaged over 5000 events. Note that in our generating procedure we do not fix the total strangeness and charge of particles in a single event. However, we have checked that fluctuations of these quantities are relatively small for typical events. In particular, absolute values of net total strangeness do not exceed 1% of  $B_{\text{tot}}$ .

### III. RESULTS

#### A. Comparison of density profiles

The process of fireball expansion into a vacuum has been simulated in parallel within the hydrodynamic and GiBUU models. In this section we compare the density profiles for different hadronic species. Figure 3 shows the nucleon and pion densities in the fireball c.m. frame. These densities are summed over different isospin states of corresponding hadrons. Histograms in Fig. 3 are obtained within the GiBUU model by using Eq. (11) for  $i = N, \pi$ . Thin lines represent the profiles of densities  $n_i \gamma$  obtained within the HDM. In the case of pions, deviations between two calculations are visible already at relatively short times  $t \lesssim 5 \text{ fm}/c$ . In particular, one can clearly see an excess of pions predicted

by GiBUU in a central region. This effect can be explained by multi-hadron absorption processes missed in GiBUU but implicitly included in the HDM. Another possible reason is the Bose-enhancement effects neglected in transport calculations, but taken into account in generating initial events (see the footnote at the end of Sec. II C). At later times the HDM densities are systematically larger than the GiBUU predictions in this region.

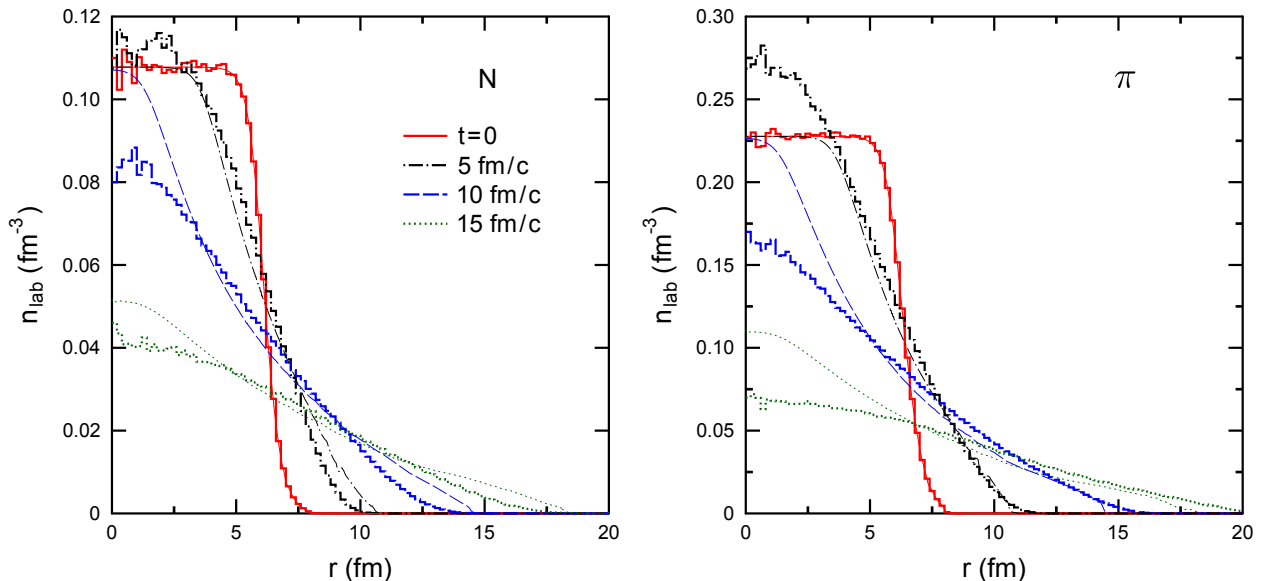


FIG. 3: The radial profiles of nucleon (left panel) and pion (right panel) densities calculated within the GiBUU (histograms) and hydrodynamic (thin lines) models.

The density profiles of  $\Lambda$  hyperons and kaons are shown in Fig. 4. One can see again that in contrast to the HDM, the particle densities in the central region increase in GiBUU at early times. However, at  $t \gtrsim 10 \text{ fm}/c$ , the local densities of  $\Lambda$ 's predicted by HDM decrease much faster with time than those obtained in GiBUU. This is a consequence of the rapid drop of the activation factor  $\exp[(\mu_\Lambda - m_\Lambda)/T]$  as the matter cools down. This factor is especially important for massive particles like hyperons and baryon resonances. As we shall see in Sect. III C a faster drop of densities gives rise to a qualitatively different time evolution of heavy particles' multiplicities in the HDM and GiBUU.

## B. Collective velocities

There is no unique way to determine a collective velocity (CV) of particles in transport models. One possibility is to define this velocity (we denote it by  $\mathbf{v}_1$ ) as the velocity of LRF

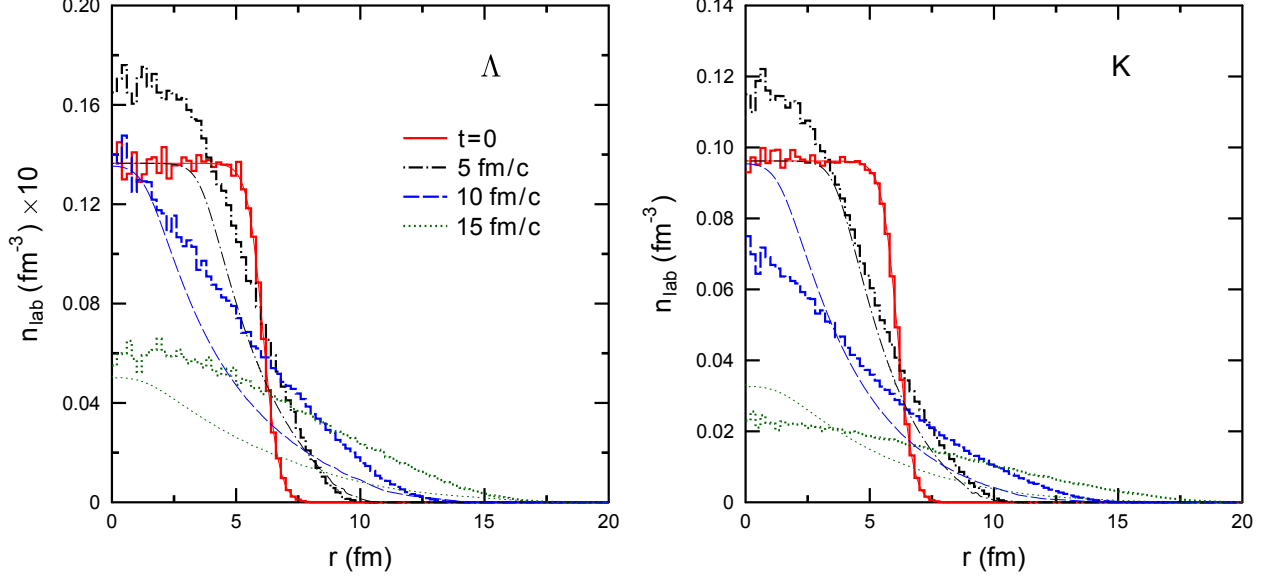


FIG. 4: Same as Fig. 3, but for radial profiles of  $\Lambda$  hyperons (left panel) and kaons (right panel).

where the 3-vector of the current density vanishes in average over many events. In the case of spherically symmetric expansion, the CV has only the radial component. In general, within GiBUU, the hadrons of different types have different CVs. Using the Lorentz transformation to the frame where the radial current of  $i$ -th hadronic species equals to zero, one obtains the relations:

$$\tilde{J}_i^r = 0 \rightarrow v_1^{(i)} = \frac{J_i^r}{J_i^0}. \quad (13)$$

The current density components in second equation are calculated by using (11).

Another possibility is to find the velocity of reference frame with vanishing 3-momentum flux. We denote the corresponding CV by  $v_2$ . From the Lorentz transformation for the energy-momentum tensor one has

$$\tilde{T}_i^{0r} = 0 \rightarrow v_2^{(i)} = \frac{2T_i^{0r}}{T_i^{00} + T_i^{rr} + \sqrt{(T_i^{00} + T_i^{rr})^2 - 4(T_i^{0r})^2}}. \quad (14)$$

It can be shown that in the case of a local equilibrium both definitions give the same values of CV:  $v_1^{(i)} = v_2^{(i)} = v$ , where  $v$  is the flow velocity in the HDM. Our GiBUU calculations show that  $v_1^{(i)}$  and  $v_2^{(i)}$  are nearly equal for all kinds of hadrons. In the following we determine the CV by using the definition (13).

The radial profiles of CV for nucleons and pions are shown in Fig. 5 for several times  $t$ . One can see that these CV are not equal to each other in the transport calculation. At small  $t$  significant differences between  $v^{(N)}$ ,  $v^{(\pi)}$  and the hydrodynamic velocity exist only at

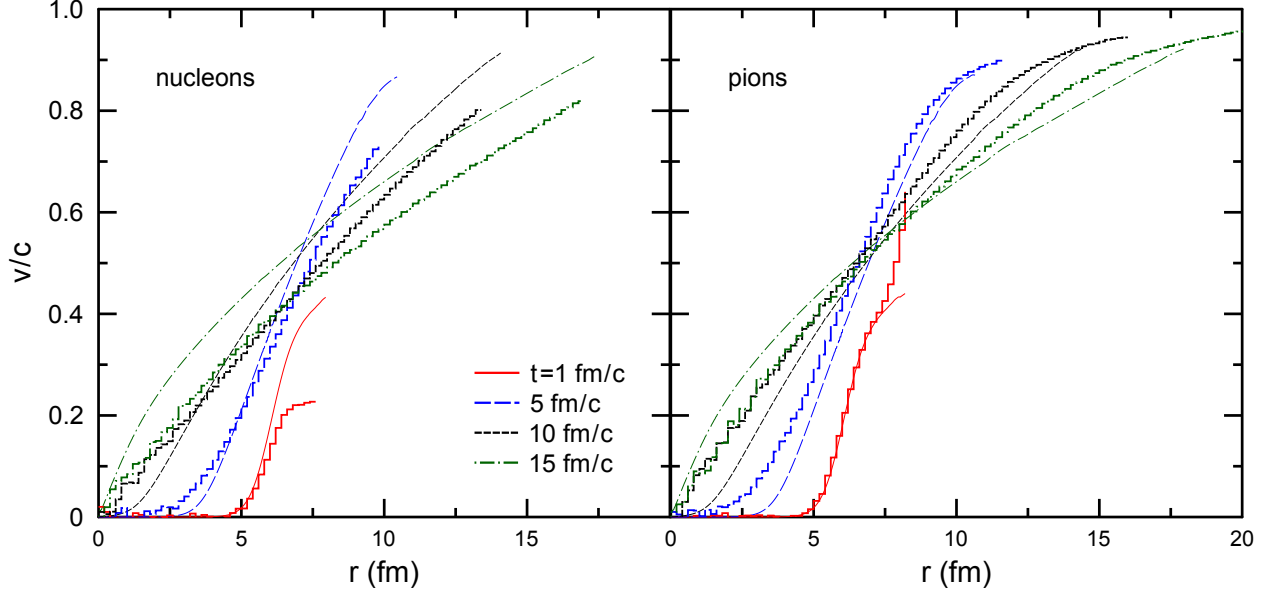


FIG. 5: Collective velocities of nucleons (left panel) and pions (right panel) as functions of radius  $r$  at different times indicated in the left panel. Thick and thin lines are calculated within the GiBUU and HDM, respectively. Outer parts of profiles corresponding to densities below  $10^{-3} \text{ fm}^{-3}$  are omitted.

the fireball periphery. At later times the differences become visible for all  $r$ . The deviations between the models are especially large for nucleons at  $t \gtrsim 10 \text{ fm/c}$ . These deviations can be explained by dissipative effects effectively included in GiBUU, but disregarded in the HDM.

### C. Hadron abundances

In this section we compare evolutions of particle multiplicities predicted by the GiBUU and HDM. These multiplicities are obtained from radial profiles of partial densities by integration over the fireball volume. In addition to the partial densities of "free" hadrons,  $n_i$ , below we also calculate the corresponding total densities,  $n_i^{\text{tot}}$ , which include hadrons "hidden" in heavier hadronic resonances [17]:

$$n_i^{\text{tot}} = n_i + \sum_j d_j^i n_j, \quad (15)$$

where  $d_j^i$  is the average number of  $i$ -th hadrons, produced in decays  $j \rightarrow i + X$ . The sum in the r.h.s. runs over all resonances included in our simulations (see Table I) and having strong decays into  $i$ -th hadrons. The coefficients  $d_j^i$  are calculated using branching ratios given in Ref. [48].

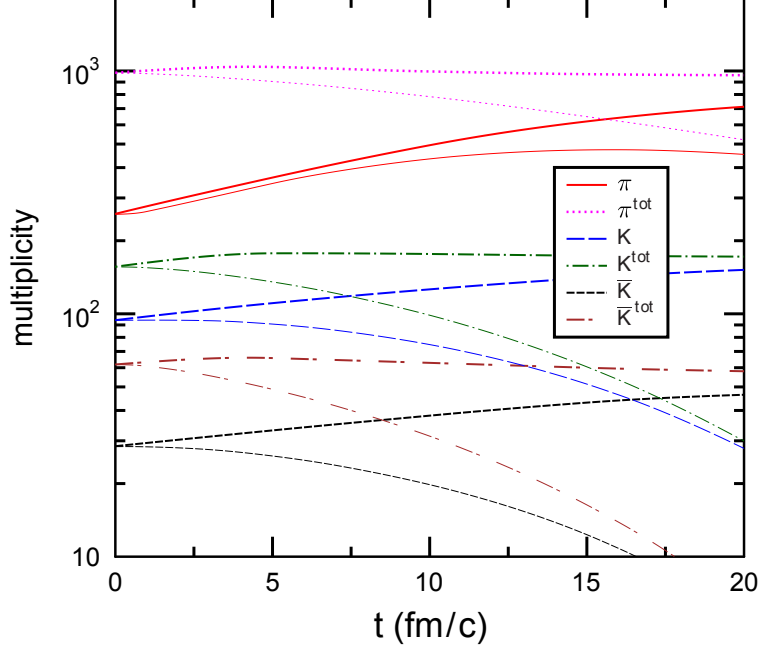


FIG. 6: Multiplicities of pions, kaons and antikaons as functions of time in the hadronic fireball expanding into vacuum. Thick (thin) lines are calculated within the GiBUU (hydrodynamic) model.  $\pi^{\text{tot}}$ ,  $K^{\text{tot}}$  and  $\bar{K}^{\text{tot}}$  are total numbers of pions, kaons and antikaons including mesons, hidden in hadronic resonances (see Eq. (15)).

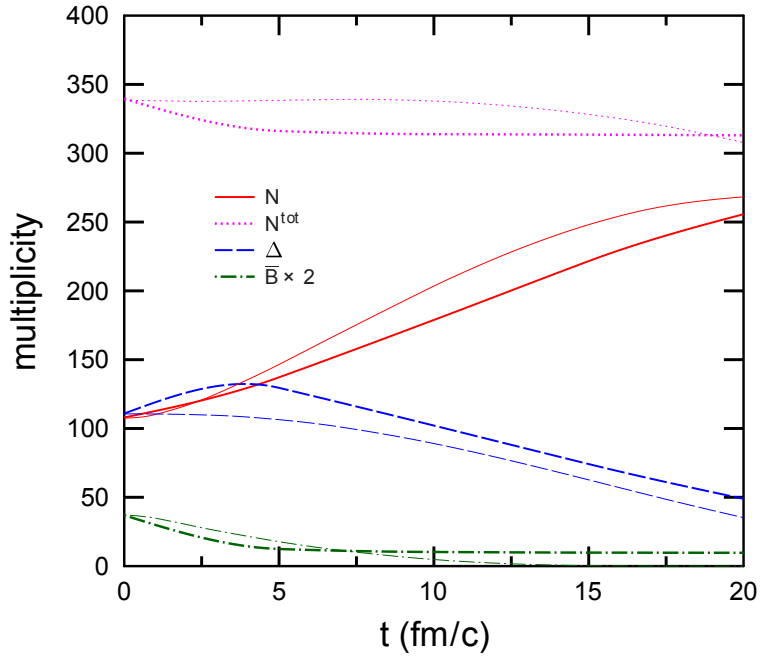


FIG. 7: Same as Fig. 6, but for nucleons,  $\Delta$ -isobars and antibaryons.  $N^{\text{tot}}$  is the total number of nucleons including those, hidden in hadronic resonances.

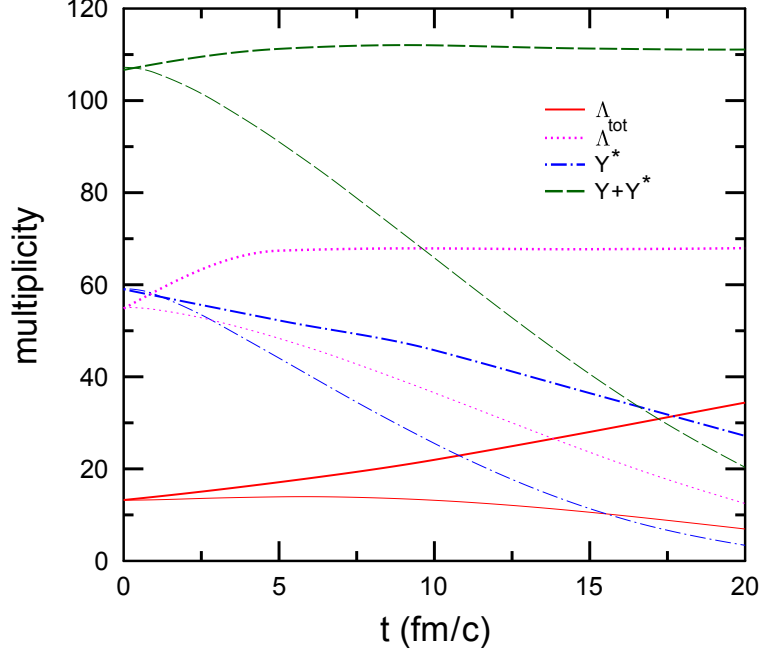


FIG. 8: Same as Fig. 7, but for multiplicities of hyperons.  $Y(Y^*)$  denote multiplicities of all stable (unstable) hyperons.  $\Lambda^{\text{tot}}$  is the total number of  $\Lambda$ 's including those, hidden in hyperonic resonances.

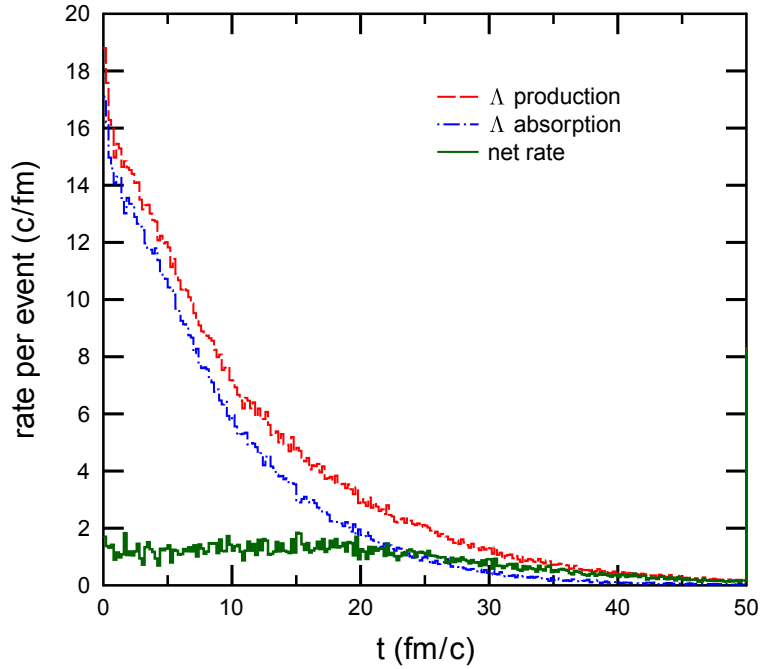


FIG. 9: Total production (dashed line) and absorption (dash-dotted line) rates of  $\Lambda$  hyperons as functions of time in GiBUU. The solid line shows the net (production minus absorption) rate.

Figures 6–8 show the time evolution of hadron multiplicities predicted by the GiBUU

and hydrodynamic models. One can see a qualitative difference between the results of two calculations. In particular, the GiBUU model predicts nearly constant total multiplicities of pions, kaons and hyperons including hadrons hidden in resonances. However, these quantities decrease noticeably within the HDM.

The two models predict very different time evolution of multiplicities of hyperons and hyperonic resonances. As one can see from Fig. 8, the multiplicity of  $\Lambda$  hyperons noticeably increases in GiBUU, but decreases in the HDM. According to our transport calculation, the number of  $\Lambda$ 's increases from 13 at  $t = 0$  to about 50 at  $t = 40$  fm/c. Within this time interval many  $\Lambda$  particles are still "bound" in hyperonic resonances. When time increases from 0 to 40 fm/c, the relative fraction of bound  $\Lambda$ 's decreases from about 80% to 30% [59]. A long duration of  $\Lambda$  production in GiBUU is directly connected with a slow decrease of the abundances of hyperonic resonances (compare dash-dotted curves in Fig. 8). This in turn follows from significant regeneration of these resonances in baryon-baryon and baryon-meson collisions.

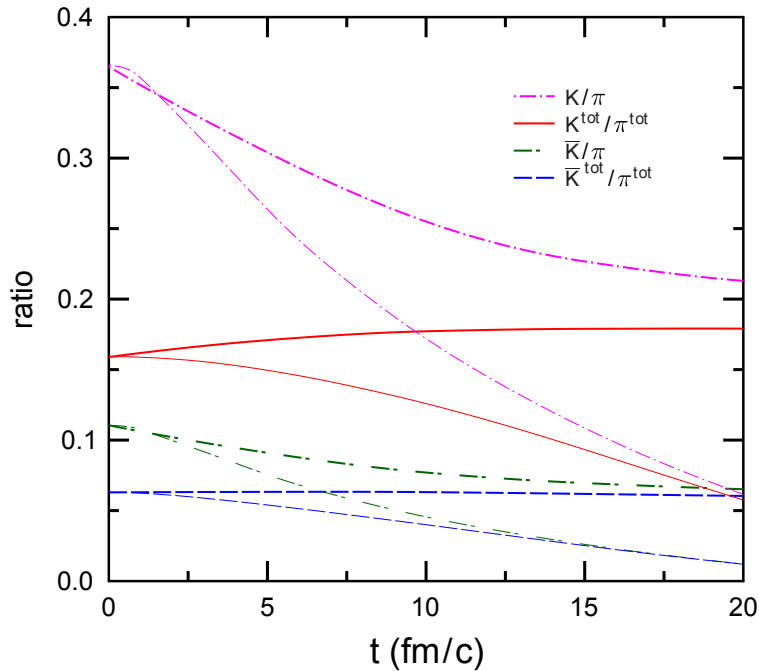


FIG. 10: (Anti)kaon to pion ratios as functions of time in expanding fireball. Thick (thin) lines are calculated within the GiBUU (hydrodynamic) model.

To analyze relative importance of different channels of  $\Lambda$  production and absorption we have calculated total rates of such processes in GiBUU. This analysis shows that for our parameters of initial state, the most important production channels are decays  $Y^* \rightarrow \Lambda M$



(here  $M$  denotes a nonstrange meson) and  $\Sigma B \rightarrow \Lambda X$ ,  $Y^* B \rightarrow \Lambda X$  reactions ( $B$  is a non-strange baryon). On the other hand, most significant channels of  $\Lambda$  absorption are the reactions  $\Lambda M \rightarrow Y^* X$  and  $\Lambda B \rightarrow (\Sigma, Y^*) X$ . As one can see in Fig. 9, both the  $\Lambda$  production and absorption rates are rather high at  $t \lesssim 20$  fm/c, but they nearly compensate each other: the net production rate is of the order of 1 c/fm at  $t \lesssim 40$  fm/c. Only later the multiplicity of  $\Lambda$  hyperons saturates. It is interesting that large characteristic times (exceeding approximately 40 fm/c) of  $\Lambda$  production have been obtained earlier in the UrQMD [11] and BUU [49] calculations.

Figure 10 shows the time dependence of (anti)kaon to pion multiplicity ratios. Again, one can see significant differences between the model predictions. For example, the ratios  $K^{\text{tot}}/\pi^{\text{tot}}$  and  $\bar{K}^{\text{tot}}/\pi^{\text{tot}}$  are practically constant in the GiBUU calculation. However, they rapidly decrease with time in the HDM. These results may imply large deviations from chemical equilibrium in expanding baryon-rich hadronic matter created at FAIR, NICA and lowest RHIC energies.

#### D. Evolution of energy distributions

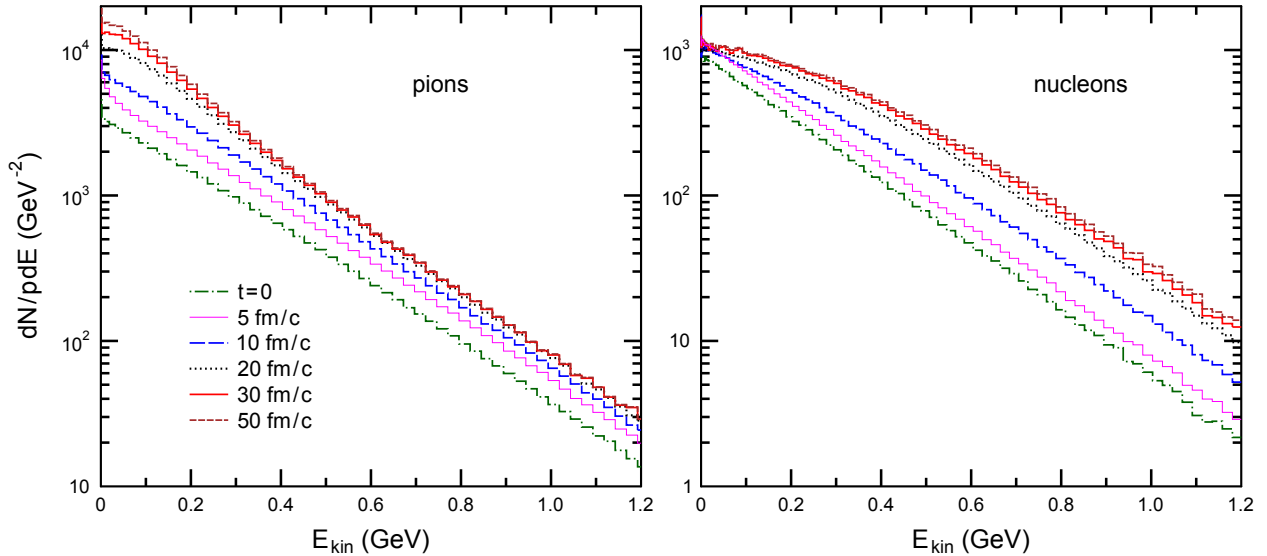


FIG. 11: Kinetic energy distributions of pions (left panel) and nucleons (right panel) in expanding fireball. Lines show the GiBUU results at different time moments  $t$ .

It is instructive to see, how particle momentum spectra evolve with time in GiBUU. In Figs. 11–12, we show the kinetic energy distributions of pions, nucleons, kaons

and  $\Lambda$  hyperons at different  $t$ . One can clearly see the importance of final state rescatterings and resonance decays in formation of these spectra. The collective expansion results in concave and convex shapes of momentum distributions for pions and nucleons, respectively. These effects are less pronounced for kaons and  $\Lambda$ 's. The GiBUU simulations predict the sequential behavior of freeze-out. Indeed, the formation of asymptotic distributions is taking place at different times for different hadrons. First, this happens for kaons (at  $t \sim 20$  fm/c),

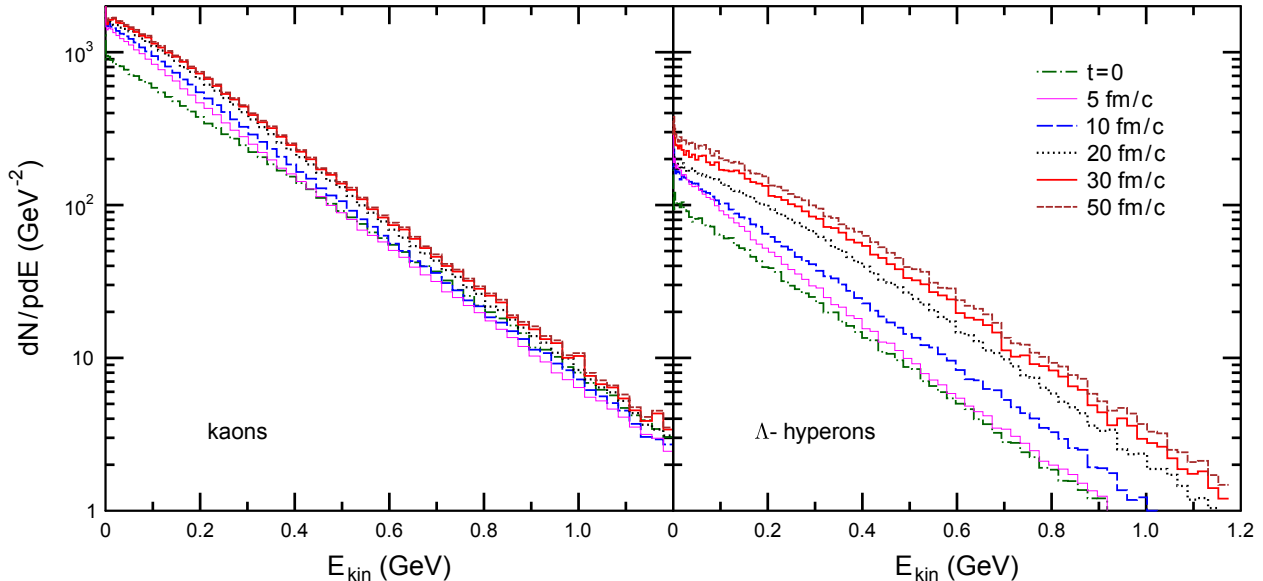


FIG. 12: Same as Fig. 11, but for kaons (left panel) and  $\Lambda$ 's (right panel).

then for pions and nucleons ( $t \gtrsim 30$  fm/c) and finally, for  $\Lambda$  hyperons ( $t \gtrsim 50$  fm/c). One can not clearly distinguish the stages of "chemical" and "thermal" freeze-out, especially for  $\Lambda$ 's.

#### IV. CONCLUSIONS

In this paper we have compared the results of transport (GiBUU) and hydrodynamic calculations for the expansion of a baryon-rich hadronic fireball. The initial events for transport calculations have been generated in accordance with locally equilibrated phase-space distributions of hadrons. We have found significant differences in space-time evolution of partial densities and collective velocities of hadrons predicted by these models. Also, the two models predict very different time evolution of hadron abundances.

The present study demonstrates that a simple picture of sequential chemical and kinetic freeze-outs is strongly distorted by the decay and regeneration of hadronic resonances.

According to our transport calculations, an early saturation of the particle multiplicities in an expanding fireball occurs only for the total yields, which include hadrons hidden in heavier resonances. This is especially important for strange hadrons. The hydrodynamic simulations with chemically equilibrated EoSs strongly underestimate total multiplicities of hyperons and kaons. We believe that strong deviations from chemical equilibrium predicted by transport calculations for such hadrons are real and they should be explicitly taken into account in future hydro–cascade calculations [60].

However, one should be very careful in selecting and combining the corresponding models. Obviously, a smooth matching of the models is only possible if there exists a stage when both transport and hydrodynamic models predict a similar behavior of macroscopic quantities. On the basis of our present analysis we conclude that these models predict an essentially different evolution of particle densities and velocities. Therefore, the combined model predictions will strongly depend on the choice of the transition hypersurface.

One should bear in mind, that in this paper we have disregarded viscosity effects in the hydrodynamic calculations. These effects may be responsible for the differences in collective velocities predicted by the two models. In the future we are going to check sensitivity of the results to the choice of initial conditions. In particular, we plan to extend our analysis to the case of nonzero initial collective velocity of the fireball. It would be also interesting to perform calculations with inclusion of relativistic mean fields. In this way one can effectively account for soft non-binary hadronic interactions disregarded in our present calculations.

## Acknowledgments

The authors thank U. Mosel for stimulating discussions, M.I. Gorenstein and E.L. Bratkovskaya for useful remarks. This work was supported the Helmholtz International Center for FAIR, by the DFG grant 436 RUS 113/957/0–1 (Germany), and the grant NSH–7235.2010.2 (Russia).

## Appendix A: Generation of initial events

In our calculations we assume that initial particles are located inside a cube with dimensions  $|x|, |y|, |z| < L$  ( $\mathbf{r} = 0$  corresponds to the fireball center). This cube is divided into smaller cells with same sizes  $\Delta l$  along each coordinate axis. Below we choose  $L = 10$  fm,

$\Delta l = 0.2$  fm. For each cell we determine average numbers of the  $i$ -th hadrons,  $\overline{N}_i = n_i(\Delta l)^3$ , where  $n_i$  is their partial density at the cell center. The latter is calculated by integrating the equilibrium DF (3) over the 3-momentum. This calculation is performed for all mesons, baryons and antibaryons listed in Table I.

It is assumed that for each hadronic type particle multiplicities in a given cell are distributed in accordance with the Poisson distribution. In this case the probability to find  $n$  hadrons of the type  $i$  in the cell is given by the expression

$$w_n^{(i)} = \frac{\overline{N}_i^n}{n!} \exp(-\overline{N}_i). \quad (\text{A.1})$$

From Eq. (A.1) one can see, that the probability that a given cell is empty, i.e. contains no hadrons, equals  $P_0 = \prod_i w_0^{(i)} = \exp(-\overline{N}_{\text{tot}})$ , where  $\overline{N}_{\text{tot}} = \sum_i \overline{N}_i$  is the total average multiplicity of hadrons of all types in the cell. For our choice of parameters,  $w_1^{(i)} \simeq \overline{N}_i \ll 1$  even for most abundant hadrons. Probabilities to find more than one hadron ( $n \geq 2$ ) are negligible for all cells. In our calculations we consider only events with cells containing no more than one hadron.

At the first step of the initialization procedure we generate randomly particle's coordinates  $x, y, z$  assuming that each coordinate is homogeneously distributed in the interval  $(-L, L)$ . Then we find the cell containing the point  $(x, y, z)$  and decide whether it is empty or not. To determine this, we choose a random number  $\xi$  with the homogeneous distribution in the interval  $[0, 1]$ . If the inequality  $\xi < 1 - P_0$  does not hold, the cell is considered empty (it is excluded from further treatment of a given event). In the opposite case we consider the cell as "filled" and generate the type of hadron contained in it [61]. Following Ref. [33] we assume that the relative probability of  $i$ -th species equals  $\overline{N}_i/\overline{N}_{\text{tot}}$ . For hadrons with nonzero isospin  $I$  we randomly generate its isospin projection  $I_3$ . This is done assuming the homogeneous distribution of  $I_3$  in the interval  $|I_3| \leq I$ .

At the second step we generate a hadronic 3-momentum  $\mathbf{p}$ . It is postulated that the momentum distribution of the  $i$ -th hadron in a given cell is proportional to the equilibrium DF introduced in Eq. (3). Normalizing this distribution to unity, one gets the relation

$$\frac{d^3 w_i}{d^3 p} = \frac{f_i^{(eq)}}{n_i} \equiv \varphi_i(\mathbf{p}). \quad (\text{A.2})$$

To generate particle's momentum in accordance with distribution (A.2), we use the well-known rejection method [53] extending it to the case of three dimensions. First, we randomly

choose three components of  $\mathbf{p}$ , assuming that each component is homogeneously distributed in the interval  $[-p_m, p_m]$  where  $p_m = 3 \text{ GeV}/c$ . Generating a new random number  $\xi \in [0, 1]$ , we accept the momentum  $\mathbf{p}$  if the inequality  $\xi < \varphi_i(\mathbf{p})/\varphi_i(0)$  holds [62].

This procedure is continued for other cells until the total net baryon number of generated particles does not exceed the value  $B_{\text{tot}}$  determined by the initial density profile  $n(r, 0)$  (see Eq. (1)). The resulting set of coordinates, momenta and types of particles is considered as a single event. It is used as an initial condition for subsequent GiBUU simulations.

- 
- [1] G.D. Westfall *et al.*, Phys. Rev. Lett. **37**, 1202 (1976).
  - [2] J.P. Bondorf, S.I.A. Garpman, and J. Zimanyi, Nucl. Phys. A **296**, 320 (1978).
  - [3] P.J. Siemens and J.O. Rasmussen, Phys. Rev. Lett. **42**, 880 (1979).
  - [4] E. Schnedermann, J. Sollfrank, and U. Heinz, Phys. Rev. C **48**, 2462 (1993).
  - [5] P. Braun-Munzinger, J. Stachel, J.P. Wessels, and N. Xu, Phys. Lett. B **344**, 43 (1995).
  - [6] J. Cleymans, D. Elliott, H. Satz, and R.L. Thews, Z. Phys. C **74**, 319 (1997).
  - [7] B. Friman *et al.* (Eds.), *The CBM physics book*, Lect. Notes Phys. **814**, Springer, 2010.
  - [8] J.P. Blaizot and J.Y. Ollitrault, Phys. Rev. D **36**, 916 (1987).
  - [9] P.F. Kolb, J. Sollfrank, and U. Heinz, Phys. Lett. B **459**, 667 (1999).
  - [10] D.Yu. Peressounko and Yu.E. Pokrovsky, Nucl. Phys. A **669**, 196 (2000).
  - [11] S.A. Bass and A. Dumitru, Phys. Rev. C **61**, 064909 (2000).
  - [12] D. Teaney, J. Lauret, and E.V. Shuryak, Phys. Rev. Lett. **86**, 4783 (2001);  
arXiv:nucl-th/0110037.
  - [13] G.A. Milekhin, Zh. Eksp. Teor. Fiz. **35**, 1185 (1958).
  - [14] F. Cooper and G. Frye, Phys. Rev. D **10**, 186 (1974).
  - [15] L.V. Bravina, I.N. Mishustin, N.S. Amelin, J.P. Bondorf, and L.P. Csernai,  
Phys. Lett. B **459**, 667 (1999).
  - [16] J. Knoll, Nucl. Phys. A **821**, 235 (2009).
  - [17] H. Bebie, P. Gerber, J.L. Goity, and H. Leutwyler, Nucl. Phys. B **378**, 95 (1992).
  - [18] J. Cleymans and K. Redlich, Phys. Rev. C **60**, 054908 (1999).
  - [19] W. Broniowski and W. Florkowski, Phys. Rev. Lett. **87**, 272302 (2001).
  - [20] D. Prorok, Acta Phys. Polon. B **40**, 2825 (2009).
  - [21] S.A. Bass *et al.*, Prog. Part. Nucl. Phys. **41**, 225 (1998).
  - [22] <http://gibuu.physik.uni-giessen.de/GiBUU>.
  - [23] O. Buss, T. Gaitanos, K. Gallmeister, H. van Hees, M. Kaskulov, O. Lalakulich,  
A.B. Larionov, T. Leitner, J. Weil, and U. Mosel, arXiv:1106.1344.
  - [24] W. Ehehalt and W. Cassing, Nucl. Phys. A **602**, 449 (1996).

- [25] W. Cassing (2005), <http://www.jlab.org/conferences/ECT/talks/Cassing.pdf>.
- [26] N.S. Amelin, L.V. Bravina, L.P. Csernai, V.D. Toneev, K.K. Gudima, and S.Y. Sivoklov, Phys. Rev. C **47**, 2299 (1993).
- [27] Z.W. Lin, C.M. Ko, B.A. Li, and B. Zhang, Phys. Rev. C **64**, 011902(R) (2001).
- [28] R. Rapp and E.V. Shuryak, Phys. Rev. Lett. **86**, 2980 (2001).
- [29] C. Greiner and S. Leupold, J. Phys. G **27**, L95 (2001).
- [30] W. Cassing, Nucl. Phys. A **700**, 618 (2002).
- [31] C. Nonaka and S.A. Bass, Phys. Rev. C **75**, 014902 (2007).
- [32] T. Hirano, U.W. Heinz, D. Kharzeev, R. Lacey, and Y. Nara, Phys. Rev. C **77**, 044909 (2008).
- [33] H. Petersen, J. Steinheimer, G. Bereau, M. Bleicher, and H. Stöcker, Phys. Rev. C **78**, 044901 (2008).
- [34] T. Biró, H.W. Barz, B. Lukács, and J. Zimányi, Phys. Rev. C **27**, 2695 (1983).
- [35] H.Z. Barz, B.L. Friman, J. Knoll, and H. Schulz, Nucl. Phys. A **484**, 661 (1988).
- [36] M.I. Gorenstein, S.N. Yang, and C.M. Ko, Phys. Lett. B **281**, 197 (1992).
- [37] I. Bouras, A. El, O. Fochler, C. Greiner, E. Molnár, H. Niemi, and Z. Xu, Acta Phys. Polon. B **40**, 973 (2009).
- [38] A.V. Merdeev, L.M. Satarov, and I.N. Mishustin, Phys. Rev. C **83**, 014907 (2011).
- [39] L.M. Satarov, M.N. Dmitriev, and I.N. Mishustin, Yad. Fiz. **72**, 1444 (2009) [Phys. Atom. Nucl. **72**, 1390 (2009)].
- [40] L.D. Landau and E.M. Lifshitz, *Fluid Mechanics* (Pergamon Press, New York, 1987).
- [41] I.N. Mishustin and L.M. Satarov, Yad. Fiz. **37**, 894 (1983) [Sov. J. Nucl. Phys. **37**, 532 (1983)].
- [42] G.S. Bisnovatyi-Kogan and M.V.A. Murzina, Phys. Rev. D **56**, 4380 (1995).
- [43] D.H. Rischke and M. Gyulassy, Nucl. Phys. A **608**, 479 (1996).
- [44] J.P. Boris and D.L. Book, J. Comp. Phys. **11**, 38 (1973).
- [45] D.H. Rischke, S. Bernard, and J.A. Maruhn, Nucl. Phys. A **595**, 346 (1995).
- [46] A.B. Larionov, I.N. Mishustin, L.M. Satarov, and W. Greiner, Phys. Rev. C **82**, 024602 (2010).
- [47] G.F. Bertsch and S. Das Gupta, Phys. Rep. **160**, 189 (1988).
- [48] K. Nakamura et al. (Particle Data Group), J. Phys. G **37**, 075021 (2010).
- [49] E.L. Bratkovskaya, W. Cassing, C. Greiner, M. Effenberger, U. Mosel, and A. Sibirtsev, Nucl. Phys. A **675**, 661 (2000).
- [50] T. Hirano and K. Tsuda, Phys. Rev. C **66**, 054905 (2002).
- [51] D. d’Enteria and D. Peressounko, Eur. J. Phys. C **46**, 451 (2006).
- [52] C. Shen, U. Heinz, P. Huovinen, and H. Song, Phys. Rev. C **84**, 044903 (2011).
- [53] G.A. Bird, *Molecular gas dynamics* (Clarendon Press, Oxford, 1976).
- [54] We disregard the isospin and Coulomb effects.
- [55] The columns labeled by  $I_i$  show isospin quantum numbers of corresponding hadrons.

- [56] Note, that, in general, the multiplicity of  $i$ -th hadrons,  $N_i$ , is a function of  $t$ .
- [57] The geometrical criterium, suggested in Ref. [47], is used for generating two-body scatterings.
- [58] Note that using the quantum Fermi and Bose distributions instead of the corresponding Boltzmann DF for initial hadrons within GiBUU is not fully consistent. Indeed, the Pauli blocking is normally included for nucleons in this model, but it is neglected in our present calculation to reduce the CPU time (one should have in mind that this blocking should be negligible at high temperatures considered here). On the other hand, the Bose-enhancement effects are completely disregarded in GiBUU.
- [59] In calculating  $\Lambda^{\text{tot}}$  we include  $\Lambda$  hyperons from the  $\Sigma^0 \rightarrow \Lambda\gamma$  decays. Without this contribution, the relative fraction of bound  $\Lambda$ 's changes from 70% to 7% in the same time interval.
- [60] In relation to this discussion we would like to mention several hydrodynamic models [50–52] which include chemical nonequilibrium effects.
- [61] We disregard the presence of cells with several hadrons of different types.
- [62] Our initialization procedure can be generalized for initial states with nonzero collective velocities. Then one should replace  $n_i$  by  $\gamma n_i$  and generate (instead of  $\mathbf{p}$ ) the corresponding momentum  $\tilde{\mathbf{p}}$  in the local rest frame.